HYDROGEN-HELIUM SHOCK RADIATION TESTS FOR SATURN ENTRY PROBES

Brett A. Cruden[(1)]

[(1)] *AMA Inc at NASA Ames, NASA Ames Research Center, MS 230-2, Moffett Field, CA 94035, E-mail:Brett.A.Cruden@nasa.gov*

ABSTRACT

This paper describes the measurement of shock layer radiation in Hydrogen/Helium mixtures representative of that encountered by probes entering the Saturn atmosphere. Normal shock waves are measured in Hydrogen-Helium mixtures (89:11% by volume) at freestream pressures between 13-66 Pa (0.1-0.5 Torr) and velocities from 20-30 km/s. Radiance is quantified from the Vacuum Ultraviolet through Near Infrared. An induction time of several centimeters is observed where electron density and radiance remain well below equilibrium. Radiance is observed in front of the shock layer, the characteristics of which match the expected diffusion length of Hydrogen.

1. INTRODUCTION

The 2013-2022 Decadal Survey for planetary exploration has identified probe missions to Uranus and Saturn as high priorities [1]. For Uranus, the entry velocities and shock-layer temperatures are low enough that radiative heating is negligible. For Saturn entries however, the radiative heating could be a significant fraction (up to 20%) of peak heating based on recent simulations, though the uncertainty in this prediction is substantial.[2] A shock tube test in the Electric Arc Shock Tube (EAST) facility was therefore constructed to examine the magnitude of shock layer radiation at conditions relevant to Saturn probes.

2. EXPERIMENTAL

The EAST facility has been described in detail in previous work [3], and is summarized here. The facility consists of a driver, a driven tube (with optional buffer section), and a dump tank. The EAST electric arc driver is conical with a 10.16 cm exit diameter and 1292 cm^3 volume. The energy for the arc discharge is supplied by a 1.2 MJ capacitor bank. The buffer is a 3 m section of 10.16 cm tube that is located between, and isolated from, the driven and driver gas. Helium gas was chosen for both the driver and the buffer so as to avoid a resonance excitation of the Hydrogen Lyman-α line. The driver and buffer pressures were 0.68 MPa (100 psi) and 67 Pa (0.5 Torr), respectively. The buffer/driven diaphragm was a 3 μm polyester sheet with thin aluminum coating. The coating was intended to reflect driver radiation, thus preventing radiative heating of the test gas, while the thinness of the diaphragm was necessary to achieve high velocity. With this diaphragm, no direct evidence of heating of the test gas by driver radiation, as reported in [6], was observed. The driver/buffer diaphragm was 0.25 mm (0.010") Mylar. The discharge voltages employed were between 21-35 kV, depending on driven gas pressure and velocity.

The driven tube diameter is 10.16 cm and the total length of the driven tube, from the main diaphragm to the dump tank, (including the buffer) is 12.5 m. Two turbomolecular pumping stations at either end of the driven tube evacuate the tube to base pressures less than 10^{-5} Torr prior to charging with the test gas. The test gas was an 89:11% mixture of H_2:He (by volume), which is the approximate composition of Saturn's atmosphere (generally accepted value is from 9.9-13.8% He [4].) The base pressure in the system after 1 minute (about the time required for the test sequence to run) of isolation is used to estimate an impurity level between 40-500 ppm, scaling inversely with the test pressure.

Shock arrival times are monitored by up to 18 high speed pressure transducers. The times of arrival in the test section are fit with a second-order polynomial, the derivative of which gives shock velocity. For these high velocities, it is found that small errors in the time of arrival detection may have significant impact on the velocity measurement. Therefore the reported velocities may have uncertainty up to ±0.4 km/s.

Radiation measurement in the EAST is made approximately 6.75 m downstream of the main diaphragm via 4 spectrometers in two vacuum optical boxes coupled to opposite sides of the test section. Magnesium fluoride (MgF_2) windows were employed in the vacuum ultraviolet, which are transparent to

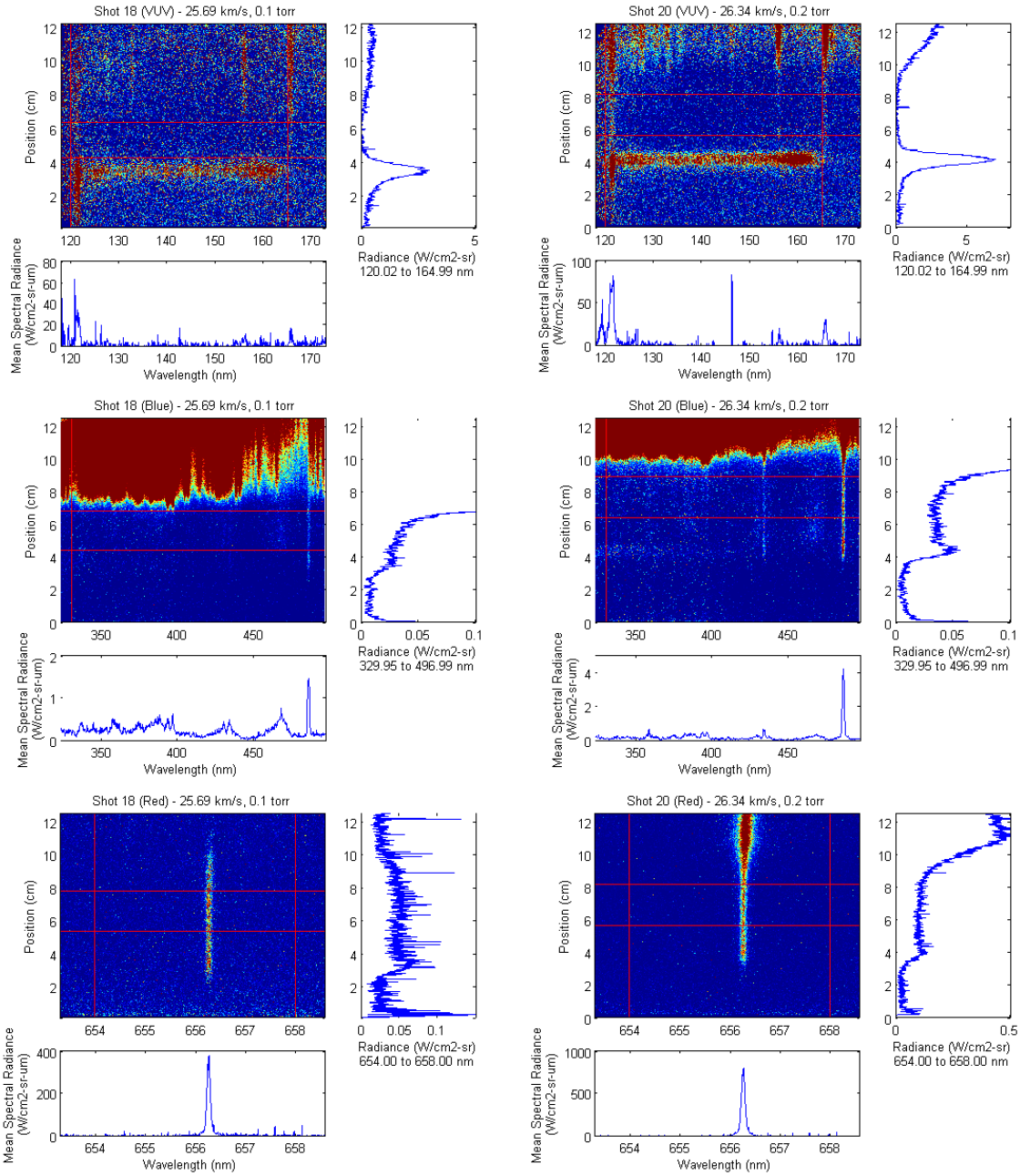

Figure 1. Test data at (left) 25.7 km/s, 0.1 Torr and (right) 26.3 km/s at 0.2 Torr. The rows represent the spectral ranges of Deep VUV, UV and Visible.

below 120 nm and could therefore measure the resonant atomic Lyman-α line and Lyman band radiation from H_2. Spectrally and spatially resolved emission from the shocked gas is thus obtained in the vacuum ultraviolet (VUV), ultraviolet (UV), visible (VIS) and near infrared (NIR). The four spectrometers are calibrated in absolute radiance units using either an integrating sphere (> 300 nm) or a D_2 lamp source (< 300 nm). The D_2 lamp source is referenced against the integrating sphere to convert relative intensities to absolute ones.

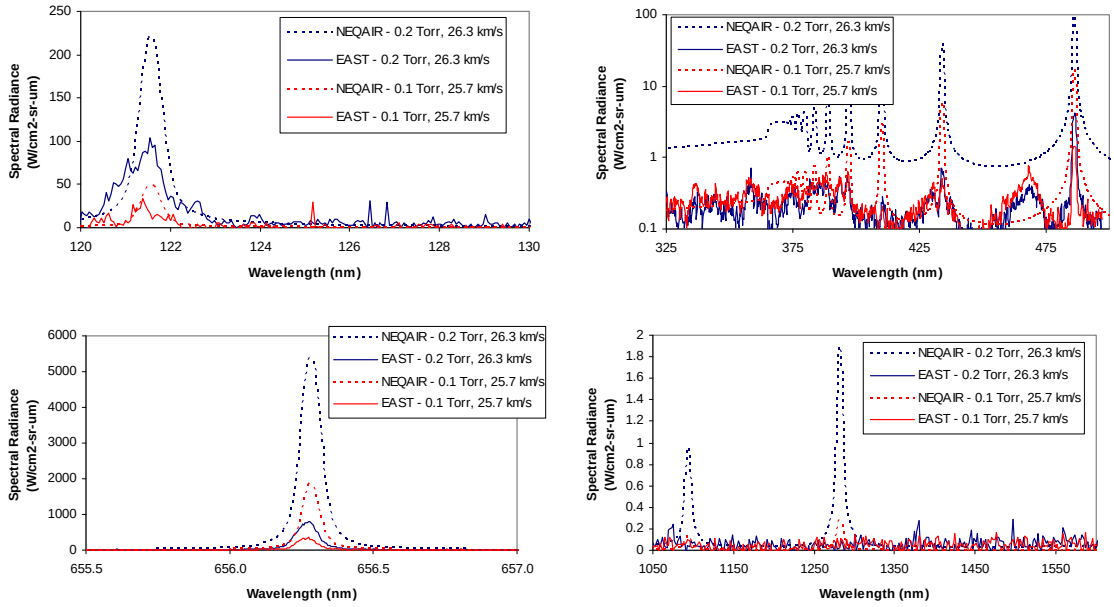

Figure 2. Comparison of EAST spectra to equilibrium radiance levels for velocities of 25.7-26.3 km/s.

3. RESULTS

A total of 25 tests were performed at pressures of 0.1, 0.2 and 0.5 Torr, three of which produced unusable data due to triggering errors, contamination or camera saturation. Of the remaining 22 tests, 6 had test time but no observable signal. These tests were all less than 25 km/s, confirming predictions that radiative heating would be negligible at these velocities. From the 16 tests with signal, test times were short or unclear in 4 of them, leaving 12 tests with high data quality. Eight of these 12 tests included measurement of the Lyman-α line in the VUV.

The data in the following is presented in order of ascending velocity. Only selected data sets are shown in this work, but the full set of data is available for download from data.nasa.gov[1].

A. 25-27 KM/S

There were four shots obtained between 25-27 km/s, including two at 0.1 Torr and two at 0.2 Torr. A representative data set is given from each of these pressures in Figure 1. The near infrared data is not shown, as any radiance was below the detection limit for these cases. The presence of the shock front is seen with a broad non-equilibrium radiance in the VUV at all conditions, near y = 4 cm. Analysis of the camera trigger and time of arrival shows that this feature actually precedes the shock front. The broad emission is attributed to the Lyman band (B-X) of molecular hydrogen, which is excited in the freestream as discussed below. The Lyman-α line at 121.6 nm is also seen and precedes the shock front by as much as 1-2 cm, with the distance being greater at lower pressure. The nature of the pre-shock radiance will be discussed in Section 4B. Evidence of Balmer continuum (or possibly molecular) emission is also faintly seen at the shock front on the UV camera. Clearer evidence of the shock front is ascertained by the appearance of the Balmer-α, β, and γ lines on the VIS and UV cameras. Following the non-equilibrium peak, the radiance settles into a steady level for several cm. The contamination is observed at about y = 8 and 10 cm at 0.1 and 0.2 Torr, respectively. This corresponds to test distances of approximately 4-6 cm.

The radiation intensities from these tests (during the valid test time) are compared against the equilibrium radiance predictions from NEQAIR/CEA for these cases in Figure 2. In the VUV, the only interesting feature expected in equilibrium is the 121.6 nm Lyman-α line, therefore only the region from 120-130 nm is shown. Both lines are somewhat below equilibrium levels, though the 25.7 km/s condition may be considered to be within the noise of the data. The UV region from 325-500 nm is shown on a logarithmic

[1] **https://data.nasa.gov/docs/datasets/aerothermodynamics/EAST/index.html, Test 56**

scale, as otherwise most features, other than the Balmer-β line (486 nm), would be difficult to observe. These features are all significantly less than equilibrium radiation levels, again suggesting that the shock has not equilibrated over the few cm of test distance. Weak molecular band features near 470, 430 and 390 nm are noted and are tentatively assigned to water impurities in the tube. The VIS camera measurement of the Balmer-α line shows a low radiance, with the peaks being 6-7× below equilibrium. There is no measurable infrared signal in these tests, even though the equilibrium levels are above the camera noise floor. The combination of these data indicates that the steady region behind the shock front is not at an equilibrium condition.

B. 27-28 KM/S

Six shots were obtained between 27-28 km/s, including three at 0.5 Torr, two at 0.2 Torr and one at 0.1 Torr. One shot from each of 0.2 Torr and 0.5 Torr conditions are shown in Figure 3. In the 0.2 Torr data (Shot 25), on all 4 cameras, the trigger was such that the shock front is near, or off of, the bottom edge of the CCD array. At 0.5 Torr (Shot 23), the shock front is near y=4 cm. The Lyman-α line again precedes the molecular emission but not by as much as at the lower pressure conditions. The contact front for Shot 25 occurs near y=8 cm and no contact front is observed in Shot 23. Due to a triggering error in the IR camera during shot 23, the near infrared data from a similar condition (Shot 22) is shown instead. Shot 22 has the shock front at y=4 cm and contact front near y=10 cm. A common feature to all these tests is a delayed radiative transition. As at lower velocity, the shock front is observed with molecular emission features in the VUV which then decay to a low value. At around 3-4 cm behind the shock front, the radiation suddenly increases. This trend is observed on all three of the VUV, UV and Visible cameras. The infrared camera shows no radiation at the shock front, but the Paschen-β and γ lines appear at the same distance where the radiation spikes on the other cameras. This radiation transition is accompanied by an increase in the atomic linewidth. The Balmer-α line at 0.5 Torr displays a flattened top, indicative of optical thickness. This delayed radiative transition, or induction time, is attributed to a relatively slow ionization rate in the shock layer. This transition was consistently observed in this testing regime, though the 0.1 Torr test did not have sufficient test time for this to occur.

The radiance following this transition is compared against equilibrium CEA/NEQAIR calculations in Figure 4. Here, the Lyman-α line exceeds equilibrium for both cases. The UV camera data is of the same order as the equilibrium computation. At 0.2 Torr, the Balmer-β line peak is somewhat above equilibrium and the γ line is somewhat below. As lines move to higher energy (lower wavelength), they become increasingly less than equilibrium. At 0.5 Torr, the peak widths are clearly wider in the experiment. Another noticeable difference between simulation and experiment is the absence of an intensity change at about 366 nm, which indicates that the Balmer continuum is not predicted correctly. The Balmer-α line, as measured by the VIS camera, is significantly wider in experiment than as given by NEQAIR. This is due to a large optical thickness at a lower effective temperature than equilibrium. The simultaneous observation of a large radiance for the $n=2\rightarrow1$ transition with a lower maximum radiance for the $n=3\rightarrow2$ transition suggests that the n=2 state is overpopulated relative to a Boltzmann distribution. In terms of the total radiative contribution (i.e. area under the curve), the experimental Balmer-α line data is in excess of equilibrium by about 35% at 0.2 Torr, but 8× larger at 0.5 Torr. The comparison in the infrared at 0.5 Torr is fairly close to equilibrium, while at 0.2 Torr, the Paschen series radiance in the infrared is slightly less than equilibrium.

The 0.2 Torr condition has shown certain lines to exceed equilibrium and others to be less than equilibrium. This trend correlates with the principle quantum number (n) of the state responsible for radiation. In excess of equilibrium are the Lyman-α (n=2), Balmer-α (n=3) and Balmer-β (n=4). Below equilibrium are the Balmer-γ and higher ($n\geq5$) and the Paschen-β and γ (n=5,6). This indicates that the electronic temperature is lower than the equilibrium shock temperature and that the shock is still equilibrating, and/or the upper states are being preferentially depopulated (e.g. by ionization) so that a Boltzmann distribution does not yet exist.

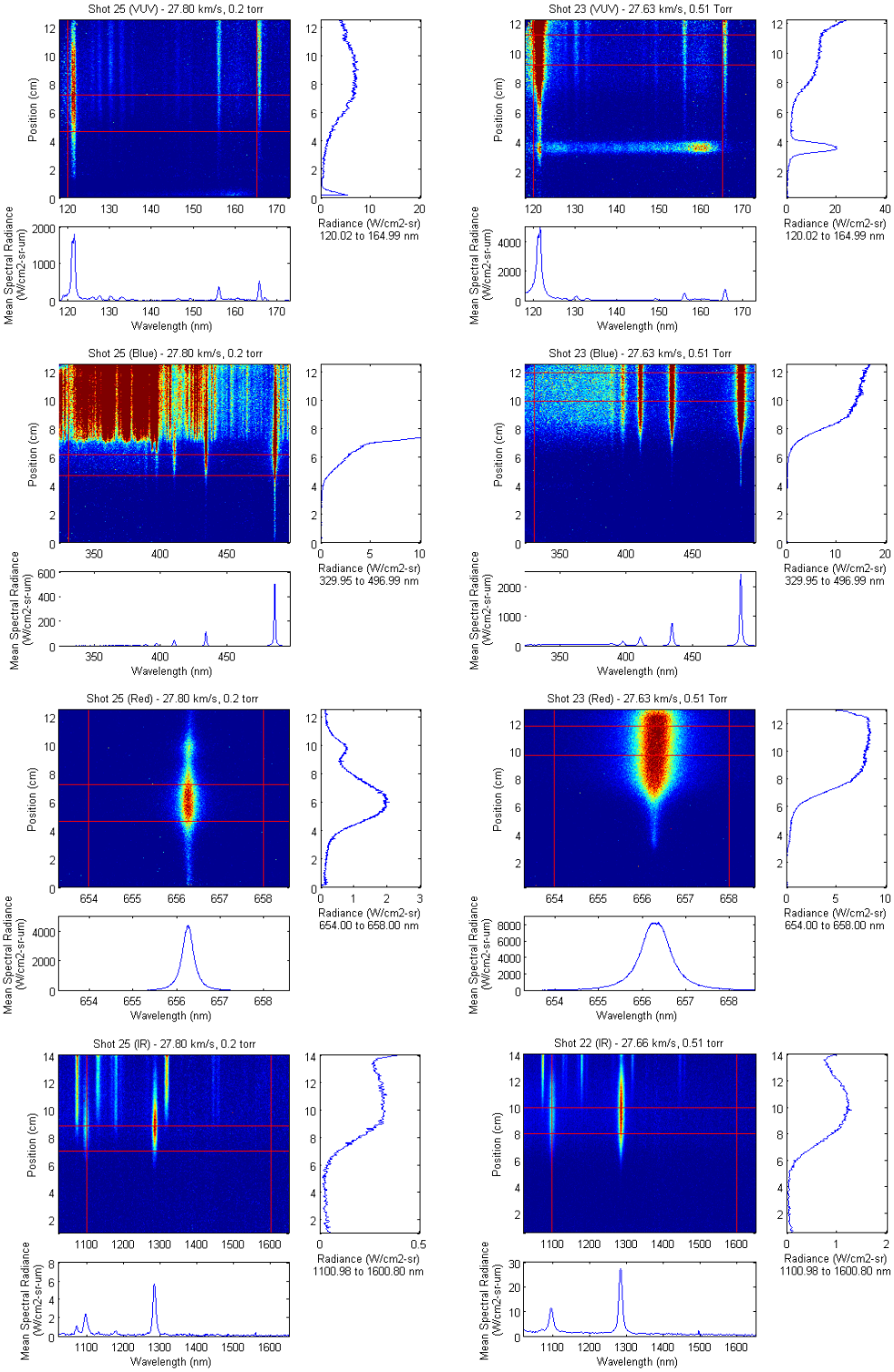

Figure 3. Data collected at (left) between 27.8 km/s and 0.2 Torr and (right) 27.6 km/s and 0.5 Torr. The rows are ordered by wavelength.

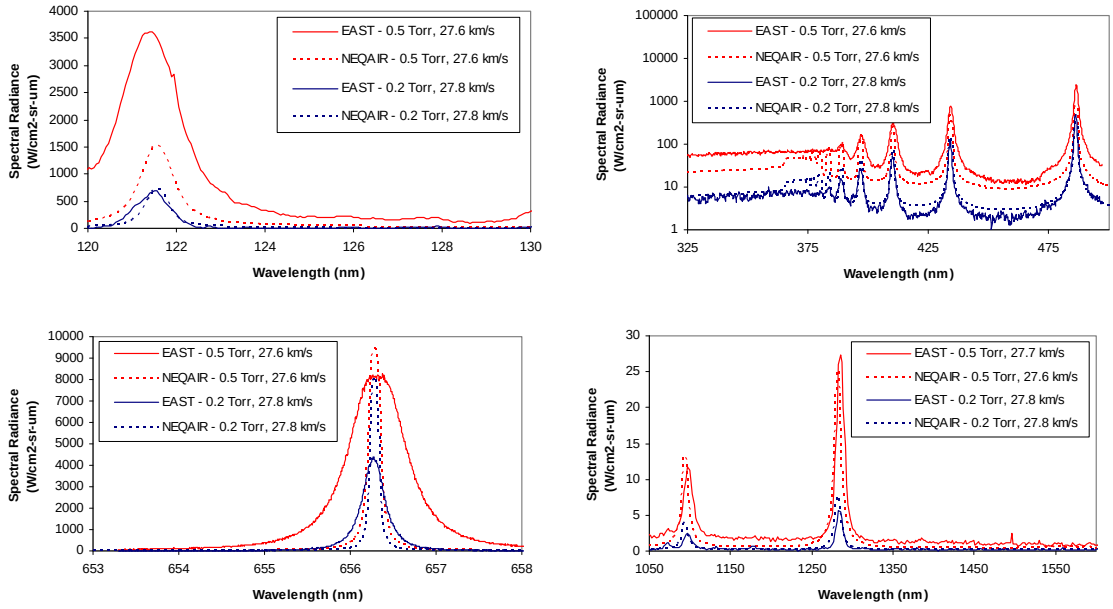

Figure 4. Comparison of 27.6-27.8 km/s to equilibrium radiance predictions.

4. DISCUSSION AND ANALYSIS

A. ELECTRON DENSITY MEASUREMENT

The spectra may be analyzed for electron density values, as discussed in our earlier work [7]. In the present work, the Balmer-α line has been measured at high resolution, and hence is preferred for Stark analysis. However, since many of the spectra are optically thick, a straight Lorentzian fit of this line may yield unrealistically high electron densities. In this case, the line shape is insensitive to electron density and instead depends on the effective temperature between the two states involved. More details, including analysis of effective temperatures is discussed in Ref. [8]. Measurements below ~10^{15} cm^{-3}. are near detection limits for the instruments, so should be taken as an upper bound to the true density. Results at 0.1 Torr are discussed in Ref. [8], only data at 0.2 and 0.5 Torr are shown here.

The electron densities at 0.2 Torr are shown in Figure 5(a). The tests are optical thick above 27 km/s, so that the α line can only be used below this velocity. The 28.7 km/s case has a test time of about 0.2 μs, so that only a few points are given. At 27.8 km/s, the density from the γ line is shown. The electron density stays low until about 3 cm behind the shock where it begins increasing. The density is still below equilibrium at the end of the test time. At 27.0 km/s, the shock becomes blackbody limited approximately 3 cm behind the shock front. Before this point, it is not entirely clear from the data whether it is blackbody limited or not. The plot shows the density from the α line until 3 cm from the shock front where it switches to the β line. The 27.0 km/s data appears inconsistent with the rest, starting to increase near 2 cm and rising above equilibrium at 3 cm. At the two lowest velocities, the density obtained from the α line is given. The 26.3 km/s data follows the same trend as at 27.8 km/s, beginning to increase at 3 cm. By the end of the test, it is at the equilibrium level. At 25.6 km/s, the electron density is near the detection limit the whole test and does not increase over the entire 5 cm.

At 0.5 Torr, all cases are blackbody limited and electron densities are found from the γ lines. The β line density is generally 1.6-1.9× lower, which is attributed to the electron density being too near the instrument linewidth. The curves are shown in Figure 5(b) and have been shifted so as to place x=0 at the estimated shock front location. The electron density curves are shown only for valid test time in Figure 5(b). At 28.8 km/s, the electron density is measured near 9×10^{15} cm^{-3} during its short test time. At 27.6-27.7 km/s, it takes about 2 cm before electron density becomes reliably detected. The density continues to rise following detection, and is near equilibrium levels at 8 cm beyond the shock front. At 27.3 km/s, the electron density is first detected near 4 cm, and

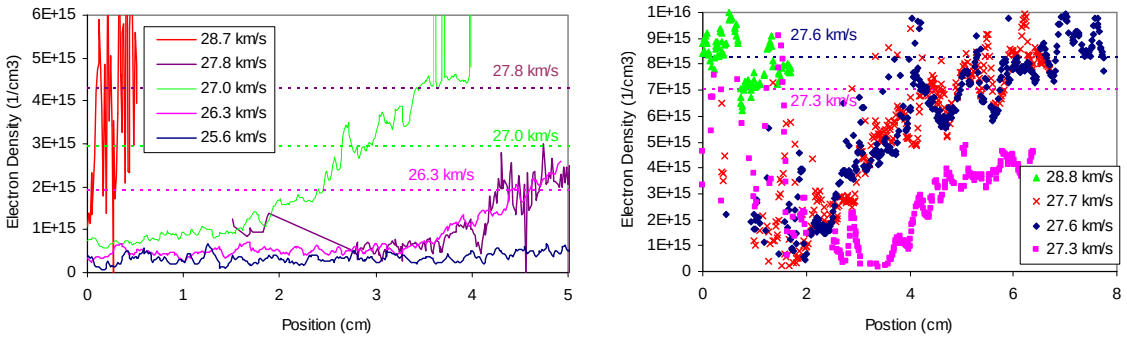

Figure 5. Electron Density deduced from H-α and/or γ linewidth at pressure of (left) 0.2 Torr and (right) 0.5 Torr. Dotted lines display equilibrium values at velocities as noted.

continues rising, but is still far from equilibrium at the end of the test almost 6 cm behind the shock front.

B. PRE-SHOCK EXCITATION

Pre-shock excitation is observed in the vacuum ultraviolet for velocities greater than 25 km/s. This includes radiation from the Lyman bands of H_2 and the Lyman-α line of H. Evidence of the pre-shock radiance is also apparent in the Balmer series. Park has recently proposed that low levels of driver radiation can excite the pre-shock region, thereby elevating the freestream energy and altering the final condition of the shocked gas [9]. However, at the same time, the heated gas may be expected to diffuse ahead of the shock front, resulting in both elevated temperatures and atom mole fractions in the pre-shock region.

These two possibilities have been evaluated through analyzing the characteristic decay lengths in front of the shock. Sample fits are shown in Figure 6 and the relaxation coefficients span between 0.3-1.0 cm for H-α and 0.2-0.5 cm for H_2 B-X, in both cases scaling inversely with pressure. A 1-D model of the pre-shock region yields an exponential decay that varies inversely with pressure for both mechanisms. For photoexcitation, the characteristic length is given as $1/\sigma_{ex}n$, where the σ_{ex} will correspond to photodissociation (for H-α emission) or photoexcitation (for B-X emission) cross-sections, and n is the H_2 density in the freestream. For diffusion, the characteristic length is D_H/v, where D_H is the diffusivity of H or H_2 and v is the shock velocity.

The equivalent excitation cross-sections are near 2 x 10^{-16} cm^2 for H-α and from 4-6 x 10^{-16} cm^2 for H_2. These decay rates are faster than expected for H_2 absorption processes, which peak at 10^{-17} cm^2 for dissociation and 10^{-16} cm^2 for excitation.[9] The diffusion coefficients are between 80-300 m^2/s for H and 40-130 m^2/s for H_2. These values match the diffusivity of H and self-diffusivity of H_2 in the freestream mixture for temperatures between about 4000-6000 K, which is between the shock and freestream temperatures. The mean free paths for a hot hydrogen atom or molecule entering the cold free-stream scale inversely with pressure from 0.13-0.66 cm and 0.05-0.25 cm, respectively. This makes the characteristic lengths equivalent to 2 mean free paths, on average.

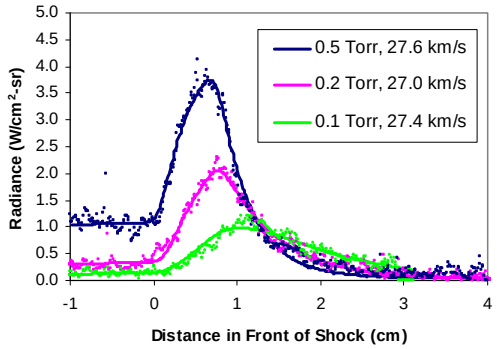

Figure 6. Radiance observed in front of the shock attributable to the Lyman-α line (120-128nm). The solid lines are fits and points are data.

The observed Lyman-α radiation is analyzed for state density. Based on the calculated absorption coefficient, the radiance is determined to be optically thick for n_H larger than 10^{12} cm^{-3} (or, equivalently, $T_e < 15{,}000K$). This corresponds to approximately 10^{-5} times the H atom density in the shock layer and 10^{-4} times the freestream density, such that only a small amount of upstream H atom is required to explain the emission magnitude.

The diffusion mechanism has recently been supported by Direct Simulation Monte Carlo (DSMC) results showing the H-atom concentrations being as high as 10^{12} cm^{-3} up to 2 cm ahead of the shock at 0.1 Torr and 1.2 cm ahead of the shock front at 0.2 Torr.[11] These atoms posses translational temperatures near 20,000K and will collide with freestream molecules at relative mean velocities of ~27 km/s. This accounts for approximately 11 eV of collisional energy which is sufficient to excite radiating states in the freestream. The current radiation models do not account for such large collisional energies at the shock/freestream interface and would need to be updated to properly predict this phenomenon, which may be a significant source of radiation. It is noted that radiative excitation of the freestream was not modeled in the aforementioned DSMC simulations. While this process appears to be too slow to explain the observed relaxation times, simultaneous modeling of the drift-diffusion and state-to-state excitation processes should be explored to understand its impact.

5. CONCLUSIONS

These tests have established conditions for future testing of Hydrogen/Helium mixtures in the EAST facility. Tests below 25.0 km/s display no radiance, as expected, due to the low temperature obtained in hydrogen. Between 25-30 km/s, radiation is observed, but equilibrium levels are not obtained over several centimeters. For most shocks, an induction time is observed, whereby radiance levels rapidly increase from low levels several centimeters behind the shock front. This sudden change in radiance is shown to coincide with an increase in electron density, and is driven by the underlying shock layer chemistry. A slow ionization rate, relative to entries in other planetary atmospheres, causes the electron density to gradually build up over the width of the shock. Radiance, particularly in the VUV, is observed in front of the nominal shock front. The characteristic distance over which the radiance persists is shown to match the ratio of diffusion to shock velocity and is approximately 2 mean free paths in the freestream. Large collisional energies at the shock/freestream interface cause excitation leading to emission signatures that would not be predicted by current modelling practices.

6. REFERENCES

1. National Research Council, Vision and Voyages for Planetary Science in the Decade 2013-2022, National Academies Press, 2012.

2. Palmer, G., Prabhu, D., and Cruden, B. A., "Aeroheating Uncertainties in Uranus and Saturn Entries by the Monte Carlo Method," Journal of Spacecraft and Rockets, Vol. 51, No. 3, 2014, pp. 801-814.

3. Cruden , B. A., "Absolute Radiation Measurements in Earth and Mars Entry Conditions," RTO-EN-AVT-218, 2014.

4. Conrath, B. J., and Gautier, D., "Saturn Helium Abundance: A Reanalysis of Voyager Measurements," Icarus, Vol. 144, No. 1, 2000, pp. 124-134.

5. Greenberg, R. B., Cruden, B. A., Grinstead, J. H., and Yeung, D., "Collection optics for imaging spectroscopy of an electric arc shock tube," Proccedings of the SPIE, Novel Optical Systems Design and Optimization XII. Vol. 7429, 2009, 74290H.

6. Bogdanoff, D. W., and Park, C., "Radiative interaction between driver and driven gases in an arc-driven shock tube," Shock Waves, Vol. 12, No. 3, 2002, pp. 205-214.

7. Cruden, B. A., "Electron Density Measurement in Reentry Shocks for Lunar Return," Journal of Thermophysics and Heat Transfer, Vol. 26, No. 2, 2012, pp. 222-230.

8. Cruden, B. A., and Bogdanoff, D. W., "Shock Radiation Tests for Saturn and Uranus Entry Probes," AIAA Paper 2015-2965.

9. Park, C., "Nonequilibrium Ionization and Radiation in Hydrogen–Helium Mixtures," Journal of Thermophysics and Heat Transfer, Vol. 26, No. 2, 2012, pp. 231-243.

10. Cruden, B. A., Brandis, A. M., and Prabhu, D. K., "Compositional Dependence of Radiance in CO2/N2/Ar Systems," AIAA 2013-2502.

11. Higdon, K. J., Cruden, B. A., Brandis, A. M., Liechty, D. S., Goldstein, D. B., and Varghese, P. L., "DSMC Shock Simulation of Saturn Entry Probe Conditions," AIAA Paper 2016-3840.

12. Park, C., "Nonequilibrium Chemistry and Radiation for Neptune Entry," Journal of Spacecraft and Rockets, Vol. 48, No. 6, 2011, pp. 897-903.

13. Matsuyama, S., Ohnishi, N., Sasoh, A., and Sawada, K., "Numerical simulation of Galileo probe entry flowfield with radiation and ablation," Journal of Thermophysics and Heat Transfer, Vol. 19, No. 1, 2005, pp. 28-35.

14. Park, C., "Stagnation-region heating environment of the Galileo probe," Journal of Thermophysics and Heat Transfer, Vol. 23, No. 3, 2009, pp. 417-424.